

Reduced Order Model of Laminar Premixed Inverted Conical Flames

L. da Costa Ramos, Florent Di Meglio, L. F. Figueira da Silva, Valéry Morgenthaler

▶ **To cite this version:**

L. da Costa Ramos, Florent Di Meglio, L. F. Figueira da Silva, Valéry Morgenthaler. Reduced Order Model of Laminar Premixed Inverted Conical Flames. 2022. hal-03604764

HAL Id: hal-03604764

https://minesparis-psl.hal.science/hal-03604764

Preprint submitted on 10 Mar 2022

HAL is a multi-disciplinary open access archive for the deposit and dissemination of scientific research documents, whether they are published or not. The documents may come from teaching and research institutions in France or abroad, or from public or private research centers.

L'archive ouverte pluridisciplinaire **HAL**, est destinée au dépôt et à la diffusion de documents scientifiques de niveau recherche, publiés ou non, émanant des établissements d'enseignement et de recherche français ou étrangers, des laboratoires publics ou privés.

Reduced Order Model of Laminar Premixed Inverted Conical Flames

Da Costa Ramos L.*
ANSYS, Villeurbanne, Rhône, 69100, France

Di Meglio F.†
MINES ParisTech, Paris, Province, 75006, France

Figueira da Silva L. F.‡
Pontíficia Universidade Católica do Rio de Janeiro, Rio de Janeiro, 22451-900, Brasil

Morgenthaler V.§
ANSYS, Villeurbanne, Rhône, 69100, France

An Inverted Conical Flame, anchored at a central bluff-body, in an unconfined burner configuration, is a flame that may be used to further understand more complex flame configurations, such as in aeronautical engines combustion chambers. This article involves the modeling of an unconfined laminar premixed ICF, anchored at a central cylindrical rod. The computational fluid dynamic modeling of this flame configuration involves the solution of transport equations of species mass, momentum and energy, which is computationally expensive. A skeletal methane/air chemical kinetic mechanism is used to capture a plethora of time and length scales. Reduced Order Models (ROM) have been shown to increase the computational efficiency of dynamical systems modeling. Accordingly, in this work a ROM of the steady ICF is developed, using the volume flow rate of the combustible mixture as input variable of the ROM, and the velocity components and the temperature fields as the output. The aim is to optimize the flame modeling computational time, thus paving the way to the reduced order modeling of acoustically excited, unstable, laminar premixed inverted conical flames. A model of the ICF has been developed with Fluent 2019 R2, and the analysis of a diversity of properties and species included in the combustion process has been made. Since a skeletal chemical kinetic model is used, the characterization of the flame is marked by its different property scales, allowing the flame front recognition over the field of CH_2. However, this CFD model does not present a static convergence behavior, but oscillates over a pseudo-steady state point. Thus an approximation of the statistical steady state has only been achieved by ensemble averaging the results. Therefore, the ROM of the ICF has been developed over a set of averaged data generated with Fluent, and its results shows agreement with CFD results, presenting an average overall error smaller than 3 **%.**

I. Introduction

Combustion and acoustic coupling is a major topic of interest for several practical systems, such as domestic boilers and gas turbines combustors, because the flame interactions with flow perturbations may lead to unstable behaviors. The design of such practical systems heavily relies on computational fluid dynamics simulation results. In cases where instabilities may arise, three-dimensional, unsteady simulations which involve dozens of chemical species are often necessary to provide an adequate system characterization [1]. Even with an ever increasing computational power, performing a large number of such detailed simulations remains unfeasible in the design phase of novel combustors. As a consequence, instability identification could occur late in the design phase, thus leading to expensive reviews.

*Research Engineer, Mechanical Engineer, louise.ramos@ansys.com
†Associate Professor, Centre Automatique et Systèmes,France/florent.di_meglio@mines-paristech.fr
‡Associate Professor, Department of Mechanical Engineering, Rio de Janeiro/luisfer@puc-rio.br and AIAA Senior Member.
§Principal Software Developer, ANSYS Research Team, France/valery.morgenthaler@ansys.com.

Lean premixed flames in low emission systems, have been shown to exhibit unstable behavior [2]. Accordingly, studies have been performed aiming to understand the physics of combustion response to incoming velocity/pressure perturbations both in laboratory flames and in combustors [3]. Indeed, investigations on flame instabilities have been carried in turbulent combustors which involve inherent geometrical complexity [4]. These studies show that mechanisms involving fuel/air ratio fluctuations triggered by pressure oscillations at the injector exhaust, vortical/flame roll up, and interactions with hydrodynamic instability modes are driving sources of unsteady motion [5].

However, laminar inverted conical premixed flames feature instability phenomena, representative of more complex situations, but in a simpler flow field framework. Such instabilities have been studied on these flames anchored on a central bluff body[2, 6]. In particular, it has been shown that these instabilities are due to velocity fluctuations on the flow, that couples with the flame and generate thermoacoustic instabilities, and that these phenomena can be controlled by forcing the system with specific frequency and velocity (u'). Thereby, studies of inverted conical flames allow to further understand the combustion coupling with acoustic in more complex engineering systems and practical cases, such as gas turbine combustors.

Studies of standard laminar conical flame dynamics instabilities have been performed [7]. However, to the best of the authors knowledge, fewer modeling studies exist concerning inverted conical flames (ICF) anchored on a bluff-body and, also, on reduced order models application to these flames, which is the aim of this paper.

Reduced order model (ROM) is a machine learning process which offers the possibility of significantly decreasing the cost of parametric exploration for complex systems. Such models are built over a few well chosen results in the design space, accurately describing the system of interest, even when large parametric excursions arise [8].

The use of ROM potentially increases the computation efficiency of the simulation of dynamical systems and it is prevalent in many physical fields [9]. A large number of techniques has been proposed for the modeling of different physical cases, such as online and offline models. Online models, which has their learning developed while measurements are being taken, have been previously studied, as for example on Neural Network applied to image recognition [10] or nonlinear Autoregressive Exogenous (NARX) Neural Network applied to solar radiation [11], and other statistic models. The offline models, which are developed over measurements that have already been obtained, first decompose the available data, using compressing techniques, such as proper order decomposition (POD) or singular value decomposition (SVD). Then a machine learning approach is applied to learn the studied system. Offline models coupled with POD have been studied on several physical systems, such as on the modeling of pressure ulcer prevention [8] and thermal behavior of fluid-cooled battery [12].

This paper is devoted to build and to characterize a reduced order model of axisymmetrical, laminar premixed flames with variable dilution by air. Willing to achieve an approximation of the unsteady ICF that has pressure fluctuations varying the flow rate, this reduced order model created has the fuel/air mixture inlet velocity as input variable for the ROM, and the flame velocity components and temperature field as output. This study is thus a first step towards the description of acoustically perturbed flames.

This manuscript is organized as follows; first the inverted conical flame is described and its scales are given. Second, the physical of the ICF and a kinetic chemical model are presented. Then, the computational model described, showing the geometry, mesh, boundary conditions and dynamic mesh adaptation, followed by an explanation of the ROM. Finally, the results from the CFD and from the ROM presented and discussed for the modeling of the static laminar premixed inverted conical flame.

II. Numerical Methodology

The studied inverted conical target flame is presented (section II.A) first, then the experimental setup is given, followed by the flame scales. Then the two used models are outlined, i.e., the computational fluid dynamics model (section II.C) and the reduced order model (section II.D).

A. Inverted Conical Flame

In this paper an axisymmetric flame, depicted at Fig. 1 is studied. In this figure the flame position is visualized by the field of OH mass fraction, which allows to verify that the laminar inverted conical flame (ICF) is anchored by a central bluff-body. Classically, the premixed flame front separates the fuel/air mixture from the combustion products. This flame has been shown to be susceptible to thermo-acoustic instabilities, mainly driven by flame convective vorticity mode [6].

1. Experimental Setup

Figure 2 shows the dimensions and boundaries of the computational domain. The ICF modeled is based on the experiments of Durox et al. [6], developed on a burner with outlet diameter of $D = 22\ mm$, represented in Fig. 2, fed with a lean methane-air mixture. The premixed fuel enters in the mixture-inlet (Fig. 2), whereas air enters in the air-inlet with a small velocity of $v_{air} = 0.3\ m/s$, so as the air flow in the domain moves downstream. The flame is anchored by a central rod with a diameter of $d = 6\ mm$ that is 2 mm higher than the burner outlet, as shown in Fig. 2. In this paper the methane/air flow has a variable volume flow rate ($\dot{\forall}_d$) and thus a variable mean flow velocity, v_d, and constant ambient pressure and temperature of 1 atm and 300 K, respectively.

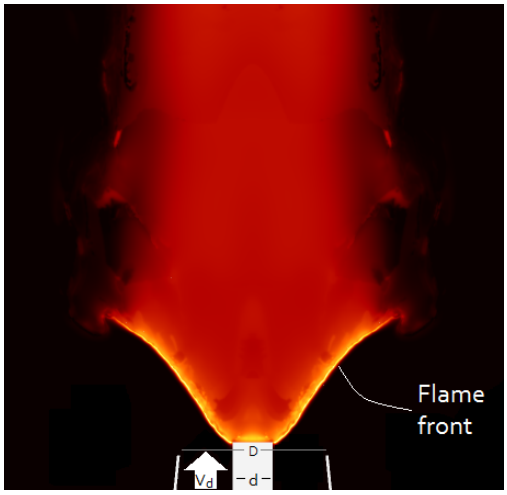


Fig. 1 Representative view of the OH mass fraction for the steady inverted conical flame (ICF). Volume flow rate of $\dot{\forall}_d = 180.3\ cm^3/s$ and fuel/air equivalence ratio $\phi = 0.92$.

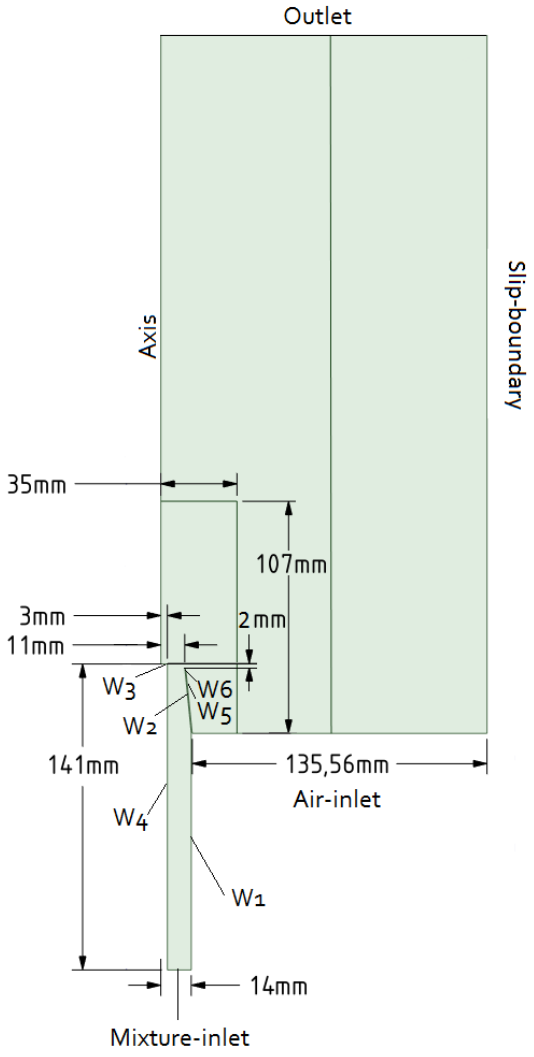


Fig. 2 Computational domain with corresponding dimensions and boundary conditions.

It is important to note that the computational domain (Fig. 2) is divided on two parts; an internal one, that includes the fuel/air inlet tube and the the combustion region, and an external one, which accounts for the air flow and the dilution of the burned gases with air. This division is used to decrease the computational burden of modeling a reactive flow on such sensible flame as the ICF. The inside part of the domain demands high cost, since it is necessary to account for the boundary layers along the bluff-body and the burner walls and, also, the reactions that arise at the flame. The dimension of this inside region have been chosen based on a preliminary trial-and-error procedure, and the boundary and mesh setup of both parts are discussed later on this paper.

2. Flame Scales

To accurately solve a premixed laminar flame, it is necessary to determine beforehand the associated scales, such as the laminar flame front speed and the thickness for the specific modeled flame. Accordingly, CHEMKIN-Pro has been used to solve an one dimensional steady premixed methane-air flame with an skeletal kinetic chemical model for the combustion (DRM19 kinetic model [13]).

The main features of the obtained solution are as follows: (1) fluid domain spanning from -2 to 5 cm, (2) an adaptive grid control based on the solution curvature and gradient threshold of 0.7 and 0.2 respectively, and (3) the laminar flame front speed S_L converged to $S_L = 40\ cm/s$. The minimum mesh size is 5.6 μm. This simple modeling with CHEMKIN-Pro using the DRM19 kinetic model, allows the analyses of diverse flame properties and its different scales. However, for the sake of brevity, three of them are discussed here only; temperature, OH and CH_2 mass fraction. This choice has been done based on the large difference between the scale of these properties both on value and lenght, which is seen at Fig. 3, and also due to the characteristics of each of the species shown. Indeed, the OH is often used for experimental flame measurements, and CH_2 is a good indicator of the flame front position and thickness. In order to examine these properties, the fields of the mass fraction of CH_2, OH and the temperature are given in Figs. 3 and 4.

One may observe that, in Fig. 3, CH_2 and OH are absent upstream to 0 cm, where the temperature is 300 K. The temperature then increases up to approximately 800 K and gives rise to the combustion, and significant amounts of CH_2 and OH may be seen. The position of the flame front is highlighted by the increase in CH_2 and OH mass fraction. Further downstream the CH_2 then is consumed and its mass fraction decreases to zero denoting the tendency to thermodynamic equilibrium. The OH, presents a maximum at the flame front, then gradually tends to an equilibrium concentration as $x \rightarrow 5\ cm$. The temperature increases along the flame until it reaches the adiabatic flame temperature, $T_{ad} = 2,200\ K$.

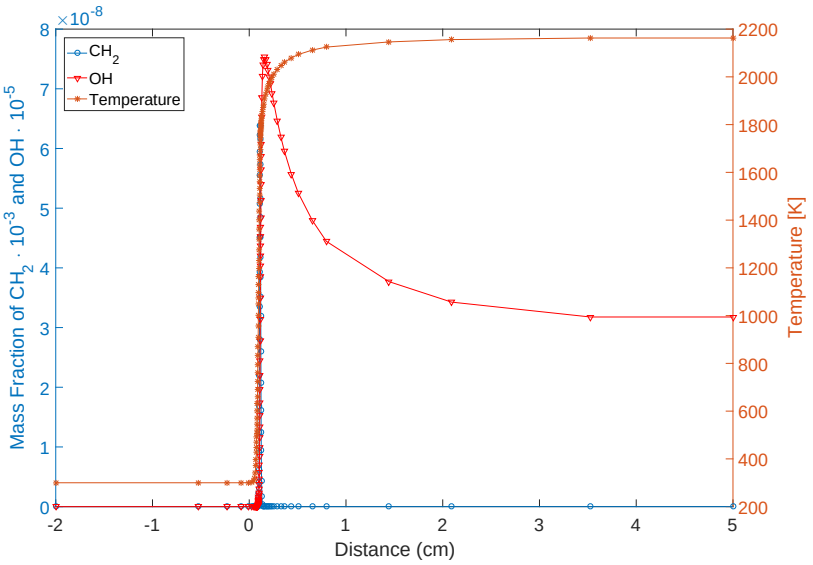


Fig. 3 Fields of mass fraction of CH_2 and OH, and temperature (K) obtained for the 1D freely propagating laminar premixed methane/air flame, with equivalence ratio of $\phi = 0.92$.

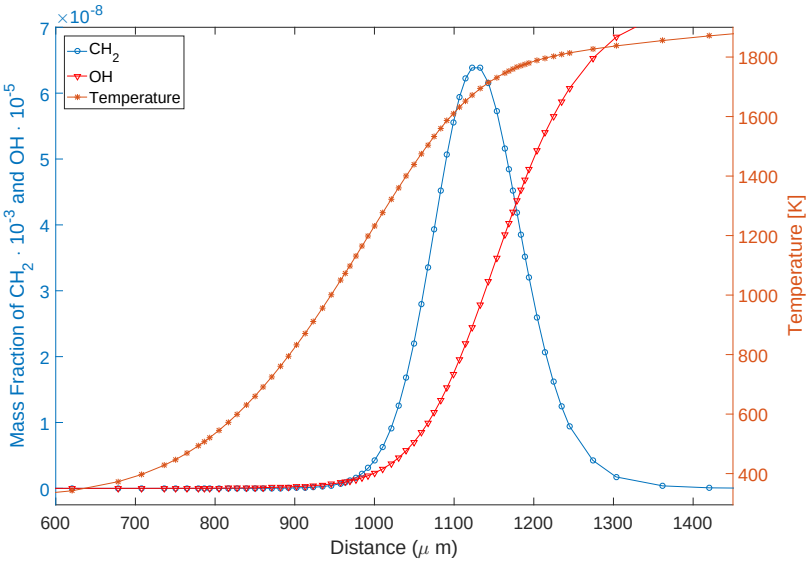


Fig. 4 Zoom on the fields of mass fraction of CH_2 and OH, and temperature (K) obtained for the 1D freely propagating laminar premixed methane/air flame, with equivalence ratio of $\phi = 0.92$.

The mass fraction profiles given in Fig. 4 indicates that the flame reaction zone thickness is around 120 μm. Also, may be inferred that the smaller mesh size required to obtain a well resolved gradient and curvature of the laminar premixed flame properties is of the order $5\mu m$, which is 24 times smaller than the flame reaction thickness.

B. Physical Chemical Model Summary

The studied flames are modeled using the transport equations of species mass, momentum and energy in an axisymmetric reference frame, since axial symmetry is believed to accurately describe the experimental results. The species mass transport equation is solved accounting for the multi-species diffusion coefficients, the Fick's law of diffusion, the Soret thermodiffusion effects, but neglecting the barodiffusion effects since the flame is isobaric. The solved energy transport equation accounts for the non unity Lewis number effects, but thermal radiation is neglected since the modeled flame is a lean premixed flame, which does not presents soot formation. Therefore, the radiative medium emission relies on CO_2 and H_2O at the burnt gases only, which is significantly smaller than the convective heat transfer contribution. As a consequence, the flame may also be considered transparent regarding the absorption process. The momentum transport equation considers the buoyancy effect, and Newtonian fluid behavior is assumed.

The chemical kinetic process for the lean methane/air mixture is described by a skeletal model. The model used is the DRM19 [13], which is a reduced GRI-Mech 1.2 kinetic model. The GRI-Mech 1.2 model is composed of 32 species and 177 reactions, which can demand a large computational cost. Because of this, a reduced model is used in this work. The DRM19 skeletal kinetic model is composed of 19 (plus N_2) species and 84 reactions [13]. Previous assessment of skeletal model accuracy supports this choice [14].

C. Computational Fluid Dynamics Model (CFD)

The numerical model of the inverted conical flame has been developed using ANSYS Fluent 2019 R2. The process of modeling a combustion problem involves the following preliminary steps: the geometry definition and the mesh generation. In this section, the most important steps to the creation of the CFD model are presented.

Since the flame is suposed to be axisymmetric, only a slice of the actual physical domain is modeled, effectively reducing the system to a 2D model, as represented at Fig. 2. The domain is composed of two surfaces with different mesh sizes, which intend to reduce the amount of computational nodes in areas where chemical reaction is absent.

The axisymmetric system has eleven boundaries, as shown at Fig. 2, where two are the rod wall and top (W_4 and W_3 respectively), two are burner internal walls (W_1 and W_2) and two are external walls (W_6 and W_5), and one represents a slip boundary ($Slip - boundary$). The remaining boundaries represent the inlets ($Air - inlet$ and $Mixture - inlet$), outlet and axis of symmetry.

The boundary conditions are applied to each boundary of the model, which is represented at Fig. 2, as follows: (1) the inlet boundaries specify the velocity, temperature and mixture molar fraction, specifically the $air - inlet$ velocity (v_{air}) is 0.3 m/s and the $mixture - inlet$ mean flow velocity (v_d) is varied from one simulation to the next, (2) the outlet boundaries specify pressure ($P_{atm} = 1\ bar$) and temperature ($T_{amb} = 300\ K$), whereas the velocity is free to vary, and (3) the wall boundaries conditions for W_1, W_2, W_3 and W_4 are no-slip, adiabatic and non catalytic, whereas W_5, W_6 and $Slip - boundary$ are slip, adiabatic non catalytic walls, since $du/dn = 0$ and $df/dn = 0$, $f = \{T, Y_i\}$. One may note that the $air - inlet$ velocity ($v_{air} = 0.3\ m/s$) is chosen based on the Froude number ($Fr = v_{air}/\sqrt{gL}$, where g is the acceleration due to gravity and L is the flame length), which might be less or equal one ($Fr \leq 1$) to allow for neglecting outer convective effects, such nonzero air velocity value is used to help the simulation convergence, since using zero air velocity led to flashback flow at the outlet boundary.

A characteristic mesh size of 100 μm is prescribed at the combustion region of the domain, i.e., inside and above the burner, and this value have been chosen smaller then the flame front thickness to assure the existence of mesh node inside of the reactive region. However, the analysis of section II.A.2 indicates that a finer mesh is required for the reactive region, indeed using a size of 5 μm throughout the flame front should be necessary, but using this mesh at the whole domain would highly increase the number of mesh nodes and, therefore, the computational burden of the simulation. For this reason, a mesh adaptation tool is applied to the model, allowing the resizing of the mesh at the regions of interest.

The mesh adaption used here is a refining and coarsening procedure used to change the mesh size based on the local temperature gradient modulus. More precisely, at the regions of the mesh where the temperature gradient is higher than 10 K/m, the mesh is refined, and in the regions of the mesh where the temperature gradient is lower than 300 K/m, the mesh is coarsened. This choice of temperature as the mesh adaptation variable is based on a trial-and-error procedure. These thresholds have been chosen by running ICF preliminary computations and analyzing the corresponding results for different meshes. Accordingly, a steady state simulation has been used with mesh adaptation at each 200, 500 and 1,000 iterations, until the convergence is achieved.

Figure 5 shows a representation of the mesh changes due to the adaption using the temperature gradient. At the left side, the figure shows the base mesh, with a size of 100 μm whereas, at the center, a representation of a mesh already adapted after the flame is developed may be seen. At the right, a zoom on the already adapted mesh is represented. A comparison between Fig. 1 and 5, shows that the mesh is refined at the flame front region, where the temperature gradient is high and the combustion process occurs. The initial regular mesh, at the left of Fig. 5, is composed of 509,473 cells, whereas the mesh, at the last instant of the simulation, presents 2,427,310 cells.

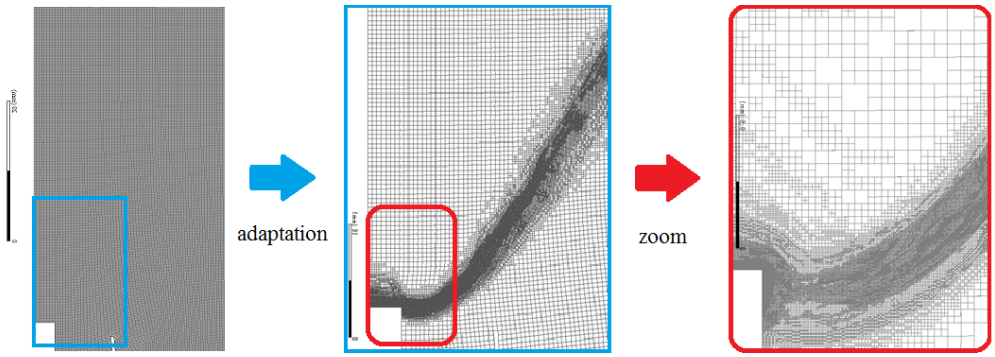


Fig. 5 Representation of the mesh adaptation due to temperature gradient (obtained using Fluent). Left: base mesh with a size of 100 μm; center: mesh already adapted after the flame is developed; right: zoom on the adapted mesh.

D. Reduced Order Model

A reduced order model (ROM) is a simplification of a high-fidelity dynamical model, used for reducing the computational burden or the storage capacity required for complex models, but preserving the essential behavior and dominant effects of the system. The ROM process is a machine learning process which has three phases; learning, validation, consumption. Here, a ROM is computed describing the relation between the mean inlet velocity (or, equivalently, volume flow rate) and the full flame velocity and temperature fields at steady state, using, as input, a

dataset generated by CFD models.

To develop a ROM, it is necessary to first choose the snapshots to compose the training set, which is used to model the system, and then divide it in two sets; i.e., the learning and the validation snapshot sets. One may note that the snapshot set is the ensemble of data available for the ROM construction, and each ROM created has its corresponding snapshot set, for instance, snapshots of temperature fields for creating a temperature ROM. Regarding the division procedure, the learning set might consist of 60 % of the available snapshots, distributed through the whole set, thus assuring that all of the ROM input variable range is included at the learning of the system, so as to avoid validation by means of extrapolation. The validation snapshots consists of the remaining 40 % of the original set.

The second step is the application of a singular value decomposition (SVD) algorithm at the learning dataset and, thus, compressing by retaining its higher modes to describe the full field only. Each of the learning snapshots corresponds to a small set of modes coefficients when projected to the reduced SVD base [8]. Then the learning process of the ROM, is done by using a Genetic Aggregation Response Surface (GARS) to interpolate the previously obtained modes coefficients with respect to the calculation parameterization [15, 16]. In sequence, the validation computes the Euclidean Norm error between the given training snapshots and the ROM results. Finally, the consumption of the developed ROM to predict the behavior of the system for different values of the input variable, inside of the parametric domain.

Here, four snapshots sets are available for the development of the ICF ROM; the first pair consists of the average velocity component fields, each composed of six or seven snapshots, respectively, whereas the other pair consists of the temperature profiles, also with six or seven snapshots respectively. All of the available snapshots have been developed with steady Fluent simulations of the ICF, with combustible mixture volume flow rates ranging from $\dot{\forall}_0 = 153.27\ cm^3/s$ to $\dot{\forall}_6 = 207.37\ cm^3/s$, evenly spaced in the parametric space. Once built, the ROM of the average velocity components and the temperature ROMs should give an accurate approximation of the solution that can be obtained with the CFD solver, but for a different set of volume flow rates.

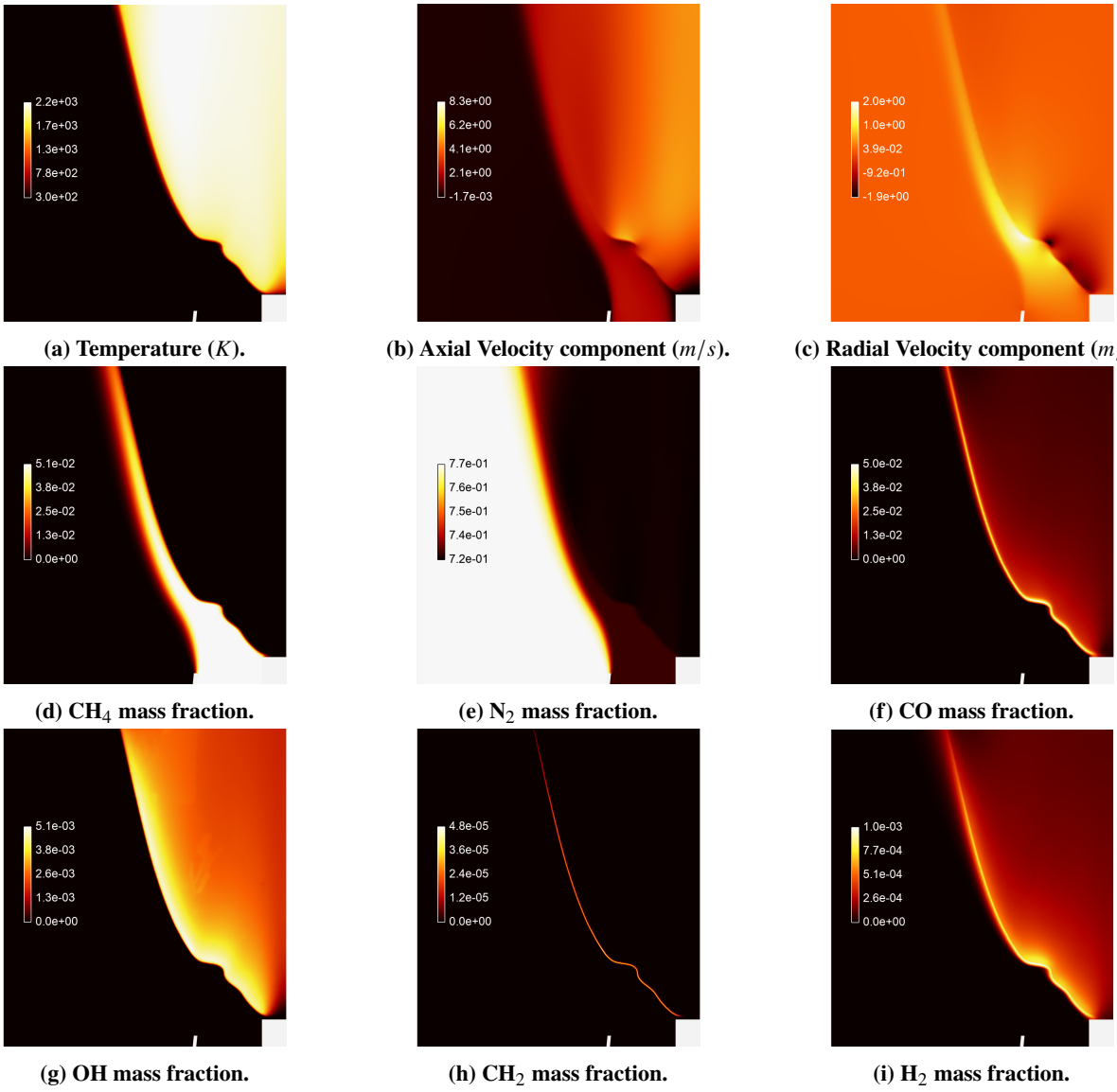
Upon the ROM process application, the resulting velocity components and temperature fields accuracy depend on the number of snapshots in the training set, the number of modes used in the field compression of the learning dataset, the statistical reduction targeted precision for the flame fields and the interpolation error.

III. Results and Discussion

In this section, results for the modeling of the inverted conical flame with Fluent and for the ROM model are presented. First, the CFD result is given and analyzed, and all of the models that have been developed in this work are listed. Then the StaticROM results for the modeling of the averaged ICF, which are developed using the CFD results as training dataset, are shown and discussed.

A. Laminar Flame Structure

In order to discuss the ICF structure, results have been obtained from the steady axisymmetric laminar premixed inverted conical flame model, with a volume flow rate of $\dot{\forall}_3 = 180.3\ cm^3/s$ and a methane/air equivalence ratio of $\phi = 0.92$. Under these reactive mixture flow conditions, the experimental results indicate that a classical premixed laminar flame is anchored at the central rod tip. This flame exhibits an inverted conical shape an gradually consumes the fuel-air mixture. Upon encountering the external air combustion is depleted. At Fig. 6, the model results are presented as a variety of the flame properties. The first three figures (Figs. 6a, 6b and 6c) exhibit the temperature and velocity components fields, whereas the others (Figs. 6d, 6e, 6f, 6g, 6h and 6i) show the mass fraction fields of selected chemical species described by the DRM19 kinetic model. These species have been shown in order to highlight the overall flame structure and, in particular, the multiple length scales that arise within the studied premixed flame.



(a) Temperature (K). **(b) Axial Velocity component (m/s).** **(c) Radial Velocity component (m/s).**

(d) CH_4 mass fraction. **(e) N_2 mass fraction.** **(f) CO mass fraction.**

(g) OH mass fraction. **(h) CH_2 mass fraction.** **(i) H_2 mass fraction.**

Fig. 6 Structure of the laminar premixed inverted conical flame, with a volume flow rate of $\dot{\forall}_d = 180.3\ cm^3/s$ and a methane/air equivalence ratio of $\phi = 0.92$.

The shape of the flame front, which is anchored at the centered bluff body, exhibits an open form, with a distinct conical shape and is visible at Fig. 6a. This figure allows to observe that the maximum temperature, $2,200\ K$, is consistent with the flame adiabatic temperature ($T_{ad} = 2,200\ K$) determined in section II.A.2. Note that the temperature at the top of the rod is constant and equal to the ambient temperature ($T_{amb} = 300\ K$). Results with different temperature values, not shown here for the sake of brevity, indicate that the heating of the rod caused by the flame does not affect with the flame anchor point nor inclination. Figs. 6b and 6c underscore the inverted conical shape of the flame, since the axial component of the velocity varies along the flame front, being approximately $v_z = 2.05\ m/s$ upstream the flame front. Due to thermal expansion, it increases immediately downstream the flame front, and the radial component increases in the region immediately upstream the flame front.

Concerning now the mass fraction of CH_4 given, at Fig. 6d, since there is ambient air flowing in the external region of the burner, at the side of the flame that is farther away from the symmetry axis, the fuel air mixture is progressively diluted by the ambient air, whereas it is consumed by the combustion reactions when it is closer to the symmetry axis. Figure 6e gives the field of mass fraction of N_2, which is present in the air and in the air-fuel mixture, with respective mass fractions of $Y_{N_2}^{air} = 0.7899$ and $Y_{N_2}^{mix} = 0.7203$. Also, farther away from the symmetry axis of the burner, N_2

mass fraction is the same of the air stream ($Y_{N_2}^{air} = 0.7899$), and as it gets closer to the flame front, the mass fraction decreases due to the dilution by CH_4. In the burner gases region, the air-fuel mixture has a mass fraction of N_2 equal to $Y_{N_2}^{mix} = 0.7203$. Downstream the flame front, the N_2 present in the fuel/air mixture is diluted by the burned gases. Figure 6f exhibits the CO mass fraction, which underscores the shape and the position of the flame front, and possibly gives an approximation of the flame thickness. Indeed, this substance is produced as the reactive region of the flame develops, and decreases after the flame front, gradually tending to the equilibrium mass fraction of $Y_{CO} = 0.0038$, at it is converted to CO_2. One may note that the field of CO approximate the flame front thickness, since this substance is not completely produced and consumed the combustion region, mixing and reacting with other burned gases downstream the flame, which could give a thickness measurement larger than other more representations.

Figure 6g gives the field of mass fraction of OH, which is produced in the reaction region and could also be an identifier for the position and shape of the flame front. Figure 6h shows the field of mass fraction of CH_2, which gives a sharp representation of the flame thickness, since it is produced and consumed within the combustion region. The model results indicates a flame thickness of approximately 130 μm, measure obtained with Fluent scaled rule, which agrees with the size of 120 μm presented at section II.A.2, and presenting an error of 8.34 %. In the field of CH_2 it is possible to see that the flame front has a size of approximately 120 μm. Finally, Fig. 6i shows the field of mass fraction of H_2, which is produced in the combustion and part of it is consumed in the reactive region.

Figure 6 illustrates the various length scales that may result of choosing a kinetic model that accounts for different species and the importance of the adaptive mesh. Included, the above discussed chemical species exhibit different physical scales, which have been accounted for by the chemical reactions represented by the DRM19 chemical kinetic model. Besides, the well resolved flame results is possible thanks to the adaptive mesh procedure, which allows to refine the mesh from a size of 100 μm to a minimum size at the flame region (5 μm), as shown in Fig. 5. This mesh size is able to capture the flame scales since it is a mesh 24 times smaller then the flame thickness.

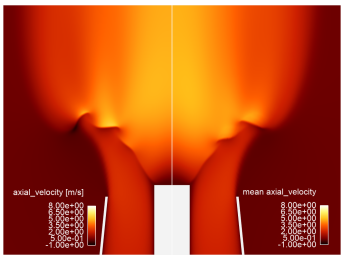
B. Learning and Validation dataset generation

A total of seven cases of the steady inverted conical flames have been simulated with Fluent 2019 R2. Each simulation took about 15 to 20 days to complete on a Linux-64 SuSE, at ANSYS cluster, Intel(R) Xeon(R) E5-2660 v3, using 108 nodes on 9 machines,. For each case, the nominal mean inlet velocity,v_i, of the premixed combustible gases is varied according to the values presented in Table 1. Such a variation of the fuel/air mixture inlet velocity is performed to generate enough ICF data for subsequent use on the ROM development. These values are chosen based on the nominal mean velocity of $v_d = 2.05\ m/s = v_3$, which has been studied in the experimental work [6], by varying the mean inlet velocity of the fuel/air mixture in 5 % multiples of the nominal velocity, v_d. On what follows the nominal mixture volume flow rate and the mean velocity values have been denoted as $\dot{\forall}_d$ and v_d, respectively.

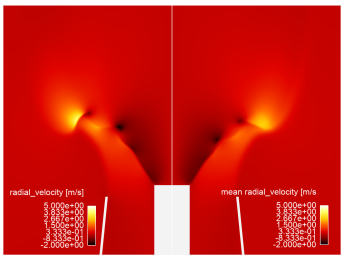
Table 1 Fuel/air mixture parameters setup for the Fluent modeling of the Inverted Conical Flame.

Case Number (i)	0	1	2	**3 [6]**	4	5	6
$\dot{\forall}_i/\dot{\forall}_d$	0.85	0.9	0.95	**1**	1.05	1.10	1.15
$\dot{\forall}_i\ [cm^3/s]$	153.27	162.29	171.30	**180.32**	189.34	198.35	207.37
$v_i\ [m/s]$	1.74	1.85	1.95	**2.05**	2.15	2.26	2.36

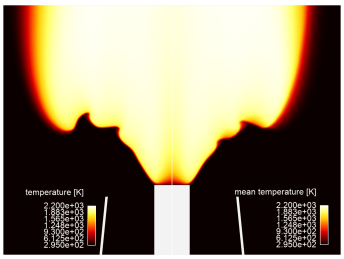
It should be emphasized that the analysis of the steady simulations shows that model does not converge strictly, but oscillates around a pseudo-steady state point. Indeed, the nine properties presented at Fig. 6 exhibit wrinkles at the flame position, and thismay possibly represent the ICF inherent instabilities, but could also be computational error related to the model. Willing to obtain an approximation of the ICF in its statistical steady state, the ensemble average of the results has been computed, in belief that this average might have a convergent behavior. Figure 7 gives the comparison between a steady snapshot and the ensemble averaged results, for the axial and radial velocity components, and temperature, for the cases with volume flow rates of $\dot{\forall}_3 = 180.32\ cm^3/s$ and $\dot{\forall}_6 = 207.37\ cm^3/s$. The purpose here is to illustrate the effect of ensemble averaging on the results. Each of these contours plots exhibit a Fluent steady snapshot result on the left, and the ensemble averaged result − over 1000 iterations − on the right side.



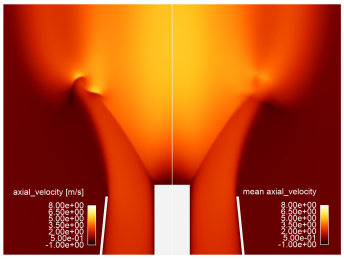
(a) Axial velocity component $[m/s]$ **for** $\dot{\forall}_3 = 180.32\ cm^3/s$**.**



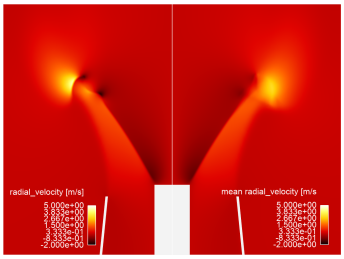
(b) Radial velocity component $[m/s]$ **for** $\dot{\forall}_3 = 180.32\ cm^3/s$**.**



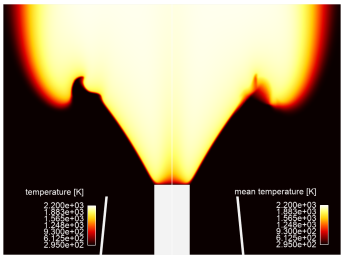
(c) Temperature $[K]$ **for** $\dot{\forall}_3 = 180.32\ cm^3/s$**.**



(d) Axial velocity component $[m/s]$ **for** $\dot{\forall}_6 = 207.37\ cm^3/s$**.**



(e) Radial velocity component$[m/s]$ **for** $\dot{\forall}_6 = 207.37\ cm^3/s$**.**



(f) Temperature $[K]$ **for** $\dot{\forall}_6 = 207.37\ cm^3/s$**.**

Fig. 7 Comparison of the flame front structure between Fluent and its average: fields of velocity components and temperature, for two different fuel/air mixture flow rates. Fluent steady snapshot on the left and ensemble average on the right side.

For the sake of brevity, the results of cases 3 and 6 are compared simultaneously. In Figs. 7a and 7d, the axial velocity component (left side) and its ensemble average (right side) are presented. These figures allow to observe that the average flame front tip, i.e., where the fuel/air mixes with the ambient air, is smeared when compared to the steady snapshot. Indeed, in the latter case the wrinkles associated to this region are smaller and smoother than those of the steady snapshot, shown at the left side of Figs. 7a and 7d. In Figs. 7b and 7e a similar behavior may be seen. Indeed, the radial velocity component presents a rather abrupt change of value on steady snapshot, whereas the averaging has, again, an smoothing effect, rendering the wrinkles weaker and smaller. The temperature fields, shown at Figs. 7c and 7f, underscore that these wrinkles at the flame front tip computed by ensemble averaging the results become smaller than those encountered on steady results. The temperature field also highlights that, even though these wrinkles at the flame tip are smeared by the averaging procedure, the flame front still preserves the overall characteristic behavior at the reactive region, such as its anchor point at the bluff-body, the flame front position, shape and length. It should also be noted that for case 6, which corresponds to the highest volume flow rate, $\dot{\forall}_6 = 207.37\ cm^3/s$, the averaging effect is even more remarkable at the flame front tip than for case 3. In particular, for case 6, the ensemble averaged flame front tip averaged velocity is rather blurred and no wrinkles are apparent.

The results shown in Fig. 7 indicate that the adopted averaging procedure allows a smoother approximation of the ICF equilibrium state when is performed a qualitative image comparison with the experimental results [6] presented in Fig. 8. It should be stressed that the flame photograph shown in Fig. 8 exhibits the natural flame luminosity, which could be associated to CH^* radicals. Such a chemical species is not presented at the DRM19 chemical mechanism, therefore, a qualitative comparison is possible only. Such qualitative comparison is not as successful as when the steady snapshot is used. These examples illustrate the importance and capacity of computing the average of CFD steady results, ensuring that the obtained model result represents the long term behavior of a system.

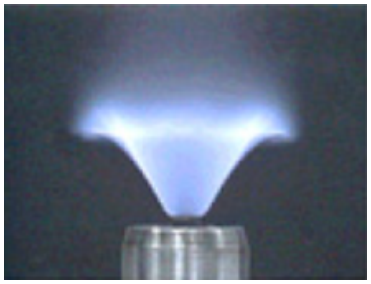
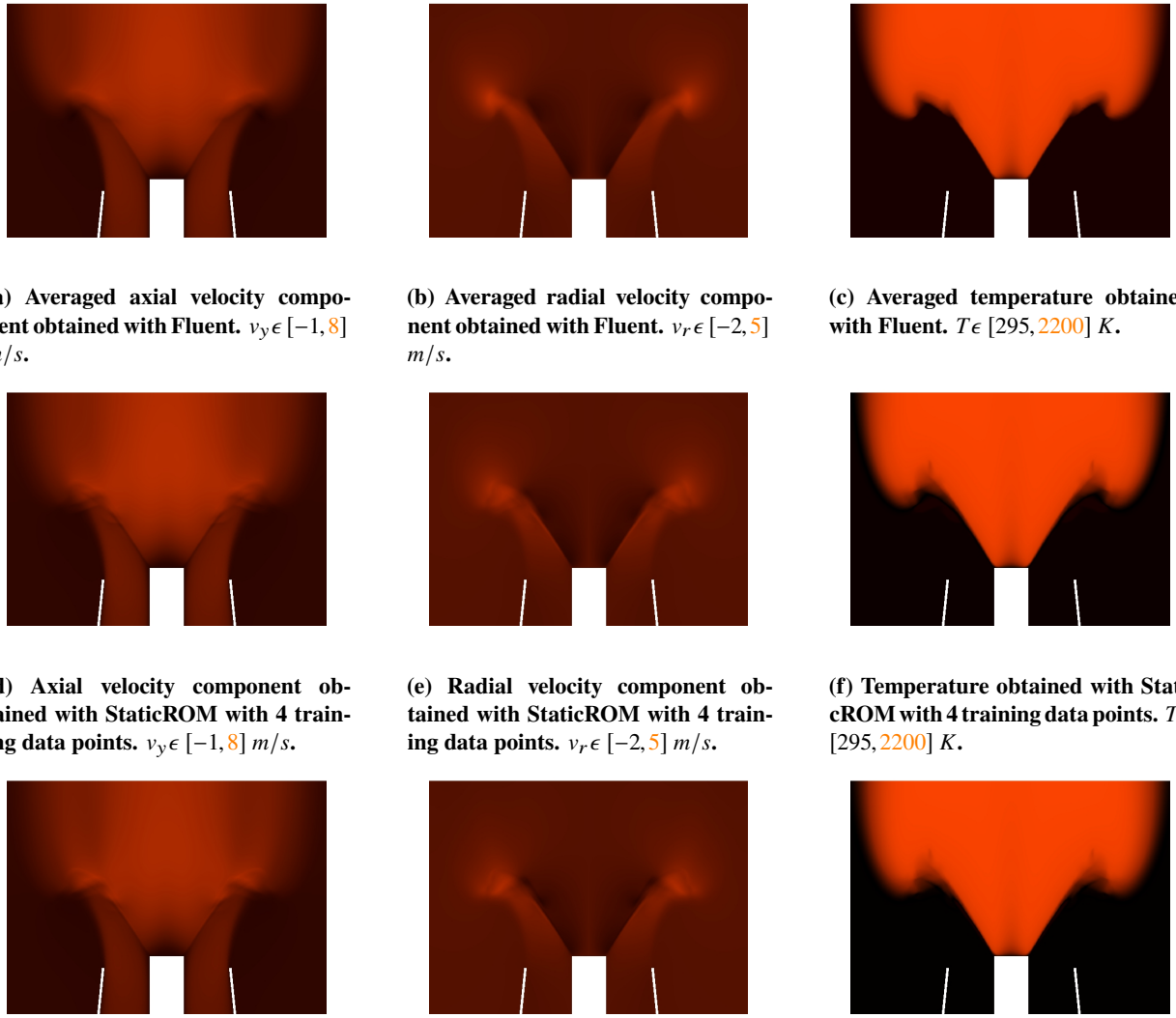


Fig. 8 Experimental steady inverted conical flame, with equivalent ratio $\phi = 0.92$ **and nominal volume flow rate** $\dot{\forall}_d = 180.32\ cm^3/s$ **[6].**

C. ROM Analysis

In order to predict the flame behavior, reduced order models have been created using some of the flame properties obtained from the ICF Fluent model results. A total of seven points are available to be used as dataset for the ROM, but the number of data points used on the learning process of this system is varied between four or five points, to show the impact of the dataset size on this process. Here, the ROM input parameter is the fuel/air mixture mean inlet velocity, v_i, which values are given, for each of the data points, in Table 1. The ROM then predicts two properties: the flame averaged velocity and averaged temperature fields.

In this study, two models are created for each of the ICF properties. The learning set of the first ROM (denoted ROM4) contains four data points (cases $1, 3, 4, 6$ in Table 1), whereas the second on (denoted ROM5) uses five points (cases $0, 1, 3, 4, 6$ in Table 1). For each ROM, cases 2 and 5 of Table 1 are used as the validation set. Figure 9 compares the Fluent averaged model results with the ROM prediction of these results, with either four or five learning points, and four SVD modes, for the velocity components and temperature fields. Table 2 reports the errors resulting from the construction of each ROM.



(a) Averaged axial velocity component obtained with Fluent. $v_y \epsilon\, [-1, 8]$ m/s**.**

(b) Averaged radial velocity component obtained with Fluent. $v_r \epsilon\, [-2, 5]$ m/s**.**

(c) Averaged temperature obtained with Fluent. $T \epsilon\, [295, 2200]$ K**.**

(d) Axial velocity component obtained with StaticROM with 4 training data points. $v_y \epsilon\, [-1, 8]$ m/s**.**

(e) Radial velocity component obtained with StaticROM with 4 training data points. $v_r \epsilon\, [-2, 5]$ m/s**.**

(f) Temperature obtained with StaticROM with 4 training data points. $T \epsilon\, [295, 2200]$ K**.**

(g) Axial velocity component obtained with StaticROM with 5 training data points. $v_y \epsilon\, [-1, 8]$ m/s**.**

(h) Radial velocity component obtained with StaticROM with 5 training data points. $v_r \epsilon\, [-2, 5]$ m/s**.**

(i) Temperature obtained with StaticROM with 5 training data points. $T \epsilon\, [295, 2200]$ K**.**

Fig. 9 Comparison between the Fluent averaged results with ROM prediction for the averaged steady ICF, for a fuel inlet volume flow rate of $\dot{\forall}_5 = 198.35\ cm^3/s$**.**

Figures 9a, 9b and 9c depict the average axial and radial velocity components, as well as temperature of the inverted conical flame with a volume flow rate of $\dot{\forall}_5 = 198.35\ cm^3/s$, modeled with Fluent. Note that, as discussed in Fig. 7, a qualitative comparison of the average field yields a smother flame front, with a shape resembling that of the steady experimental results [6]. The Static ROM result of the averaged ICF, for a volume flow rate of $\dot{\forall}_5 = 198.35\ cm^3/s$, is given in Figs. 9d, 9e and 9d for ROM4, which uses 4 training data points, and in Figs. 9g, 9h and 9g shows the results for ROM5, which uses 5 training data points.

A first qualitative comparison between the ROM and Fluent results allow to verify that the overall flow structure is correctly captured when either four or five training points are used. These: important flow structures are; (1) the flame anchoring point at the top of the rod, (2) the angle of the ICF, which is directly related to the laminar flame speed, (3) the location of the smeared flame wrinkles, that marks the dilution region and (4) the outer plume region. More precisely, at Figs. 9d and 9g, the axial velocity, v_y , upstream to the flame front is equal for both cases, with a value of $v_y = 2.34\ m/s$ and to $v_y = 4.2\ m/s$ immediately after the flame front. However, at the dilution region, the ROM velocity

goes from $v_y = 2.34\ m/s$ to $v_y = 4.6\ m/s$, since at this region the flame front is smoother and thicker. Concerning the radial velocity component, v_r, at Figs. 9e and 9h, abrupt changes are seen on the reactive region, varying from $0.9\ m/s$ upstream the flame, to $v_r = -0.9\ m/s$ immediately after the flame front, and then slowly increases, achieving a value of $v_r = 0\ m/s$ further downstream.

The temperature, given at Figs. 9f and 9i, increases from $T_{amb} = 300\ K$, to $T_{ad} = 2200\ K$. Furthermore upstream and downstream the flame front, similar Fluent and ROM behaviors are observed. However, at the dilution region, the ROM flame front is slightly different from the Fluent model. Indeed, the upper region has a flame tip smoother when compared with Fig. 9c.

The analysis of the ICF fields predicted by ROM underscores that the temperature is the available predicted property which allows to better identify the flame front position. Indeed, the interface between T_{amb} and T_{ad} is a well defined surface, both for the averaged Fluent and the reduced order models. Therefore, the temperature contour of ROM5, which uses 5 learning data points, for $\dot{\forall}_5 = 198.35\ cm^3/s$, presented on Fig. 10, is used to further understand and compare the flame front position and inclination angle. Figure 10 depicts the temperature contour for the Fluent averaged result in red, and the ROM prediction in yellow. One may note that both curves are anchored at the same position i.e., at the top of the bluff-body. Nevertheless, this figure clearly shows that the Static ROM model, created using five learning data points, is not sufficient to predict the flame front position without error. Indeed, further along the flame, at the dilution region by external air, the red and yellow lines stop overlapping, and exhibit different angles. The measure of these angles in relation to the vertical axis has been approximated by a protractor and are; 28.13° for the Fluent (red) result, and 30.38° for the StaticROM (yellow curves). This value discrepancy corresponds to a total error of 8 % for the ROM result of the flame front angle.

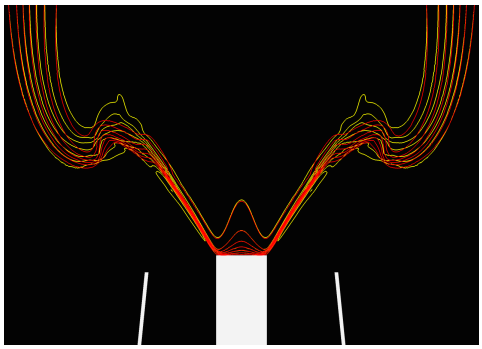


Fig. 10 Comparison of the contour of the flame temperature for the ensemble averaged steady Fluent result (red) and the StaticROM (yellow) prediction for the ICF case 6, with a volume flow rate of $\dot{\forall}_5 = 198.35\ cm^3/s$.

Tables 2 summarize the quantitative prediction capabilities of the ROM developed in this work. For each property field, the corresponding average RMS error of the SVD decomposition of the training set, and Euclidean norm error of the ROM prediction is computed. In Table 2, the prediction of the velocity components shows that the reduction error is zero for the all the properties predicted by ROM4 (ensemble average velocity $\bar{v}$ and temperature $\bar{T}$), which is evident, since the SVD is done over four learning points, and the number of modes used for the ROM is the maximum available, four also. When increasing the number of points, this table allows to verify that the reduction error increases, since the SVD is computed over five learning data points, but only the four largest modes are used on the ROM.

Table 2 RMS errors of the SVD and ROM Euclidean norm errors of the learning using 4 modes, for each of the developed models.

	SVD		ROM	
Number of learning data points	$\bar{v}_{error}$ (%)	$\bar{T}_{error}$ (%)	$\bar{v}_{error}$ (%)	$\bar{T}_{error}$ (%)
4	0	0	2.560	1.028
5	0.558	0.762	2.470	1.262

Examining now the errors given for the velocity components, in Table 2, the average ROM Euclidean norm error decreases from 2.560 % to 2.470 % when adding only one point to the learning set, which underscores the flame similarities that has been discussed previously for the comparison between ROM4 (Figs. 9d and 9e) and ROM5 (Figs. 9g and 9h). The temperature prediction average ROM, however, slightly increases from 1.028 % to 1.262 % when changing from four to five learning data points, which also agrees with the high similarity encountered on Figs. 9f and 9i, since the error is less then 2 % for both cases, for the temperature prediction on ROM4 and ROM5.

It should be also emphasized that each of the reduced order models results presented above has been computed in real time, taking around 30 s for the prediction of each created of the ROM. Nevertheless, as underscored in section III.A, a CFD simulation takes about 15 days to compute. This represents a very significant advance on the modeling of

flames in an accessible, fast and less expensive way. Furthermore, all the obtained ROM exhibit a rather small error, i.e., less than 3 %, even though a set of 5 data points has been used only.

IV. Conclusions and Perspectives

In this section the conclusions about the steady CFD and reduced order modeling of an inverted conical flame will be presented, and also the next steps towards the dynamic modeling ICF will be listed.

The steady modeling of the inverted conical flame presented on this work, developed with Fluent 2019 R2, shows that it is possible to compute for such complex reactive system, allowing the study of a diverse quantity of species by modeling the chemical of the system with skeletal kinetic models. One may note that the ICF Fluent modeling allows to delve in to the mechanics of flames, enabling a thorough analysis of different physical properties, such as miscellaneous reactive substances (i.e., CH_2, OH and H_2), which can not be achieved experimentally. Also, it has been shown that this flame setup is highly sensible, since the model does not converge to steady point exactly, but oscillates around a pseudo-steady state point. Indeed, the ICF model presents a better convergence behavior when a ensemble average of the steady results is computed. These analysis represents significant advance on the study of combustion, since it yields a characterization of these processes. However, this kind of models have a large inherent cost, that is expressed on the large number of machines necessary for computations and the amount of time required to solve complex physical system.

From the reduced order model analyses, it has been seen that its application on the modeling of the inverted conical flame is not only possible, but also beneficial. Using this type of modeling provides a substantial reduction on the computational burden linked to the modeling of combustion. The ROM developed in this work lead to less than 3 % Euclidean norm ROM error. One may also note that these models are developed using a small amount of data points for learning and validation of the ROM. Since the ICF is a complex and sensible system, the increase of the number of points on the data set could provide even better results.

The successful modeling of the steady inverted conical flame open doors to the development of dynamic study of this system, which is the perspective of this work. Since the creation and validation of the ICF model, either on Fluent and ROM, has now been complete, the modeling of the dynamics of the flame will be developed using ANSYS Software. The next step of this study is first to characterize the structure of the ICF, by means of unsteady Fluent, and use the generated data to train a dynamic ROM.

Acknowledgments

This project has received funding from the European Union's Horizon 2020 research and innovation programme under grant Agreement nr 766264. This work was performed while L.F. Figueira da Silva was on leave from the Institut Prime (CNRS, France). The authors also gratefully acknowledge the support provided by Conselho Nacional de Desenvolvimento Científico e Tecnológico, CNPq, under the Research Grant No. 403904/2016-1.

References

[1] Shinjo, J., Mizobuchi, Y., and Ogawa, S., "Numerical simulation of flame behavior in a lean premixed gas turbine combustor," *Combustion and Noise Control*, edited by G. D. Roy, Cranfield University Press, Cranfield, UK, 2003, p. 9.

[2] Birbaud, A. L., Durox, D., Ducruix, S., and Candel, S., "Dynamics of Confined Premixed Flames Submited to Upstream Acoustic Modulations," *Procedings of the Combustion Institute*, Vol. 31, 2007, pp. 1257–1265. doi:10.1016/j.proci.2006.07.122.

[3] Noiray, N., Durox, D., Schuller, T., and Candel, S., "A Unified Framework for Nonlinear Combustion Instability Analysis Based on the Flame Describing Function," *Journal of Fluid Mechanics*, Vol. 615, 2008, pp. 139–167. doi:10.1017/S0022112008003613.

[4] Lieuwen, T., and McManus, K., "Combustion Dynamics in Lean-Premixed Prevaporized (LPP) Gas Turbines," *Journal of Propulsion and Power*, Vol. 19, No. 5, 2003, pp. 721–721. doi:10.2514/2.6171.

[5] Milosavljevic, V. D., "Pertubation in Combustor Near-Field Aerodynamics as a Main Source of Thermoacoustic Instabilities in Modern Industrial Dry Low NO_x Gas Turbine Combustion Systems," *Combustion and Noise Control*, edited by G. D. Roy, Cranfield University Press, Cranfield, UK, 2003, pp. 55–60.

[6] Durox, D., Schuller, T., and Candel, S., "Combustion Dynamics of Inverted Conical Flames," *Procedings of the Combustion Institute*, Vol. 30, 2005, pp. 1717–1724. doi:10.1016/j.proci.2004.08.067.

[7] Schuller, T., Ducruix, S., Durox, D., and Candel, S., "Modeling Tools for the Prediction of Premixed Flame Transfer Functions," *Proceedings of the Combustion Institute*, Vol. 29, 2002, pp. 107–113. doi:10.1016/S1540-7489(02)80018-9.

[8] Luboz, V., Bailet, M., Boichon Grivot, C., Rochette, M., Diot, B., Bucki, M., and Payan, Y., "Personalized Modeling for Real-Time Pressure Ulcer Prevention in Sitting Posture," *Journal of Tissue Viability*, Vol. 27, 2007, pp. 1571–1583. doi:10.1002/fld.1365.

[9] Xiao, D., Fang, F., Buchan, A. G., Pain, C. C., Navon, I. M., and Muggeridge, A., "Non-intrusive Reduced Order Modelling of the Navier–Stokes Equations," *Computer Methods in Applied Mechanics and Engineering*, Vol. 293, 2015, pp. 522–541. doi:10.1016/j.cma.2015.05.015.

[10] LeCun, Y., Bengio, Y., and Hinton, G., "Deep Learning," *Nature*, Vol. 521, 2015, pp. 436–444. doi:10.1038/nature14539.

[11] Boussaada, Z., Curea, O., Ahmed, R., Camblong, H., and Mrabet-Bellaaj, N., "A Nonlinear Autoregressive Exogenous (NARX) Neural Network Model for the Prediction of the Daily Direct Solar Radiation," *Energies*, Vol. 11, 2018, p. 620. doi:10.3390/en11030620.

[12] Asgari, S., Hu, X., Tsuk, M., and Kaushik, S., "Application of POD plus LTI ROM to Battery Thermal Modeling: SISO Case," *SAE International Journal of Commercial Vehicles*, Vol. 7, 2014, pp. 278–285. doi:10.4271/2014-01-1843.

[13] Kazakov, A., and Frenklach, M. (eds.), *Reduced Reaction Sets based on GRI-Mech 1.2*, <http://combustion.berkeley.edu/drm/>, Berkeley, CA 94720-1740, USA, 1984.

[14] Celis, C., and Figueira da Silva, L. F., "Computational assessment of methane-air reduced chemical kinetic mechanisms for soot production studies," *Journal of the Brazilian Society of Mechanical Sciences and Engineering*, Vol. 38, No. 8, 2016, pp. 2225–2244. doi:10.1007/s40430-016-0494-x, URL `https://doi.org/10.1007/s40430-016-0494-x`.

[15] Acar, E., "Various Approaches for Constructing an Ensemble of Metamodels Using Local Measures," *Structural and Multidisciplinary Optimization*, Vol. 42, No. 6, 2010, pp. 879–896. doi:10.1007/s00158-010-0520-z.

[16] Viana, F. A. C., Haftka, R. T., and Steffen, V., "Multiple Surrogates: How Cross-Validation Errors Can Help Us to Obtain the Best Predictor," *Structural and Multidisciplinary Optimization*, Vol. 39, No. 4, 2009, pp. 439–457. doi:10.1007/s00158-008-0338-0.